arXiv:1612.03412v1 [cs.LG] 11 Dec 2016

Non-Redundant Spectral Dimensionality Reduction

Yochai Blau and Tomer Michaeli
Technion–Israel Institute of Technology
{yochai@campus,tomer.m@ee}.technion.ac.il

Abstract

Spectral dimensionality reduction algorithms are widely used in numerous domains, including for recognition, segmentation, tracking and visualization. However, despite their popularity, these algorithms suffer from a major limitation known as the "repeated Eigen-directions" phenomenon. That is, many of the embedding coordinates they produce typically capture the same direction along the data manifold. This leads to redundant and inefficient representations that do not reveal the true intrinsic dimensionality of the data. In this paper, we propose a general method for avoiding redundancy in spectral algorithms. Our approach relies on replacing the orthogonality constraints underlying those methods by unpredictability constraints. Specifically, we require that each embedding coordinate be unpredictable (in the statistical sense) from all previous ones. We prove that these constraints necessarily prevent redundancy, and provide a simple technique to incorporate them into existing methods. As we illustrate on challenging high-dimensional scenarios, our approach produces significantly more informative and compact representations, which substantially improve visualization and classification tasks.

1. Introduction

The goal in nonlinear dimensionality reduction is to construct compact representations of high dimensional data, which preserve as much of the variability in the data as possible. Such techniques play a key role in diverse applications, including recognition and classification [20, 2, 12, 27], tracking [24, 38, 23], image and video segmentation [40, 28, 21], pose estimation [11, 29, 33], age estimation [17], spatial and temporal super-resolution [7, 28, 5], medical image and video analysis [13, 34, 4] and data visualization [37, 25, 41, 15].

Many of the dimensionality reduction methods developed in the last two decades are based on spectral decomposition of some data-dependent (kernel) matrix. These include, *e.g.*, Locally Linear Embedding (LLE) [30], Laplacian Eigenmaps (LEM) [1], Isomap [35], Hessian Eigenmaps (HLLE) [9], Local Tangent Space Alignment (LTSA) [42], Diffusion Maps (DFM) [8], and Kernel Principal Component Analysis (KPCA) [32]. Methods in this family differ in how they construct the kernel matrix, but in all of them the eigenvectors of the kernel serve as the low-dimensional embedding of the data points [19, 3, 36].

A significant shortcoming of spectral dimensionality reduction algorithms is the "repeated eigen-directions" phenomenon [14, 16, 10]. That is, successive eigenvectors tend to represent directions along the data manifold which were already captured by previous ones. This leads to redundant representations that are unnecessarily larger than the intrinsic dimensionality of the data. To illustrate this effect, Fig. 1 visualizes the two dimensional embeddings of a Swiss roll, as obtained by several popular spectral dimensionality reduction algorithms. It can be seen that in all the examined methods, the second dimension of the embedding carries no additional information with respect to the first. Specifically, although the first dimension already completely characterizes the position along the long axis (angular direction) of the manifold, the second dimension is also a function of this axis. Progression along the short axis (vertical direction) is captured only by the third eigenvector in this case (not shown). Therefore, the representation we obtain is 50% redundant: Its second feature is a deterministic function of the first and thus superfluous.

In fact, the redundancy of spectral methods can be arbitrarily high. To see this, consider for example the embedding obtained by the LEM method, whose kernel approximates the Laplace-Beltrami operator on the manifold. The Swiss-roll corresponds to a two dimensional strip with edge lengths L_1 and L_2. Thus, the eigenfunctions and eigenvalues (with Neumann boundary conditions) are given in this case by

$$\phi_{k_1 k_2}(x_1, x_2) = \cos\left(\frac{k_1 \pi x_1}{L_1}\right) \cos\left(\frac{k_2 \pi x_2}{L_2}\right), \quad (1)$$

$$\lambda_{k_1 k_2} = \left(\frac{k_1 \pi}{L_1}\right)^2 + \left(\frac{k_2 \pi}{L_2}\right)^2, \quad (2)$$

for $k_1, k_2 = 0, 1, 2, \ldots$, where x_1 and x_2 are the coordinates along the strip. Ignoring the trivial function

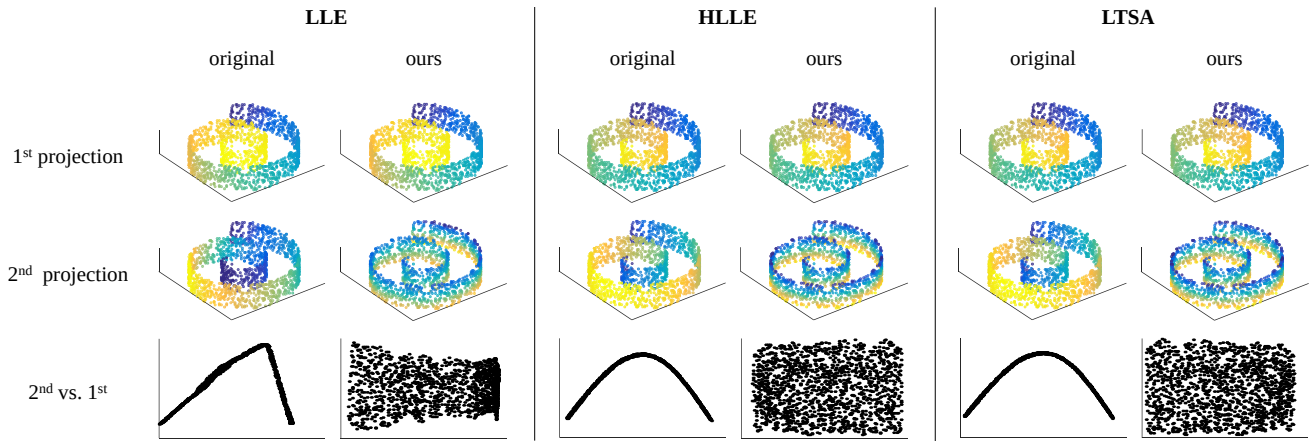

Figure 1. The first two projections of data points lying on a Swiss roll manifold, as obtained with the original LLE, HLLE and LTSA algorithms and with our non-redundant versions of those algorithms. *Top row:* The points colored by the first projection. *Middle row:* The points colored by the second projection. As can be seen, the original algorithms redundantly capture progression along the angular direction twice. In contrast, in our versions of those algorithms, the second projection captures the vertical direction. *Bottom row:* Scatter plot of the 2nd projection vs. the 1st. In the original algorithms, the 2nd projection is a function of the 1st, while in our algorithms it is not.

$\phi_{0,0}(x_1, x_2) = 1$, it can be seen that the first $\lfloor L_1/L_2 \rfloor$ eigenfunctions (corresponding to the smallest eigenvalues) are functions of only x_1 and not x_2 (see Fig. 2). Thus, at least $\lfloor L_1/L_2 \rfloor + 1$ projections are required to capture the two dimensions of the manifold, which leads to a very inefficient representation when L_1 is much larger than L_2. In fact, projections $2, \ldots, \lfloor L_1/L_2 \rfloor$ are all functions of projection 1, and are thus redundant. For example, when $L_1 > 2L_2$, the first two eigenfunctions are $\phi_{1,0}(x_1, x_2) = \cos(\pi x_1/L_1)$ and $\phi_{2,0}(x_1, x_2) = \cos(2\pi x_1/L_1)$, which clearly satisfy $\phi_{2,0}(x_1, x_2) = 2\phi_{1,0}^2(x_1, x_2) - 1$. Notice that this redundancy appears despite the fact that the functions $\{\phi_{k_1 k_2}\}$ are orthogonal (being eigenfunctions of a self-adjoint positive definite operator). This highlights the fact that *orthogonality does not imply non-redundancy*.

The above analysis is not unique to the LEM method. Indeed, as shown in [16], spectral methods produce redundant representation whenever the variances of the data points along different manifold directions vary significantly. This observation, however, cannot serve to solve the problem as in most cases the underlying manifold is not known a-priori.

In this paper, we propose a general framework for eliminating the redundancy caused by repeated eigen-directions. Our approach applies to all spectral dimensionality reduction algorithms, and is based on replacing the orthogonality constraints underlying those methods, by unpredictability ones. Namely, we restrict subsequent projections to be unpredictable (in the statistical sense) from all previous ones. As we show, these constraints guarantee that the projections be non-redundant. Therefore, once a manifold dimension is fully represented by a set of projections in our method, the following projections must capture a new direction along the manifold. As we demonstrate on several challenging high-dimensional data-sets, the embeddings produced by our algorithm are significantly more informative than those learned by conventional spectral methods.

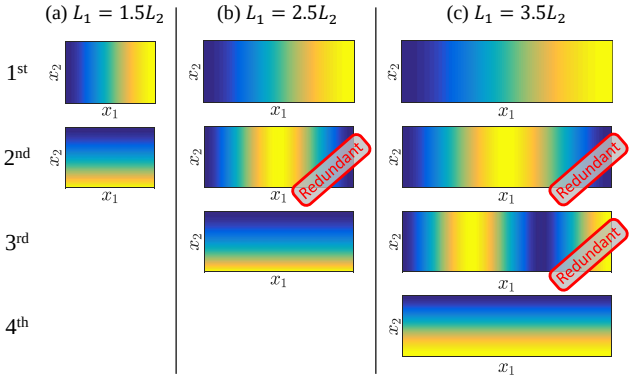

Figure 2. A 2D strip with edge lengths (a) $L_1 = 1.5L_2$, (b) $L_1 = 2.5L_2$ and (c) $L_1 = 3.5L_2$, colored according to the first few coordinates of the Laplacian Eigenmaps embedding (the eigenfunctions of the Laplace-Beltrami operator). Coordinates $2, \ldots, \lfloor L_1/L_2 \rfloor$ are redundant as they are all functions of only x_1, which is already fully represented by the first coordinate.

2. Related Work

Very few works suggested ways to battle the repeated eigen-directions phenomenon. Perhaps the simplest approach is to identify the redundant projections in a post-processing manner [10]. In this method, one begins by computing a large set of projections. Each projection is then

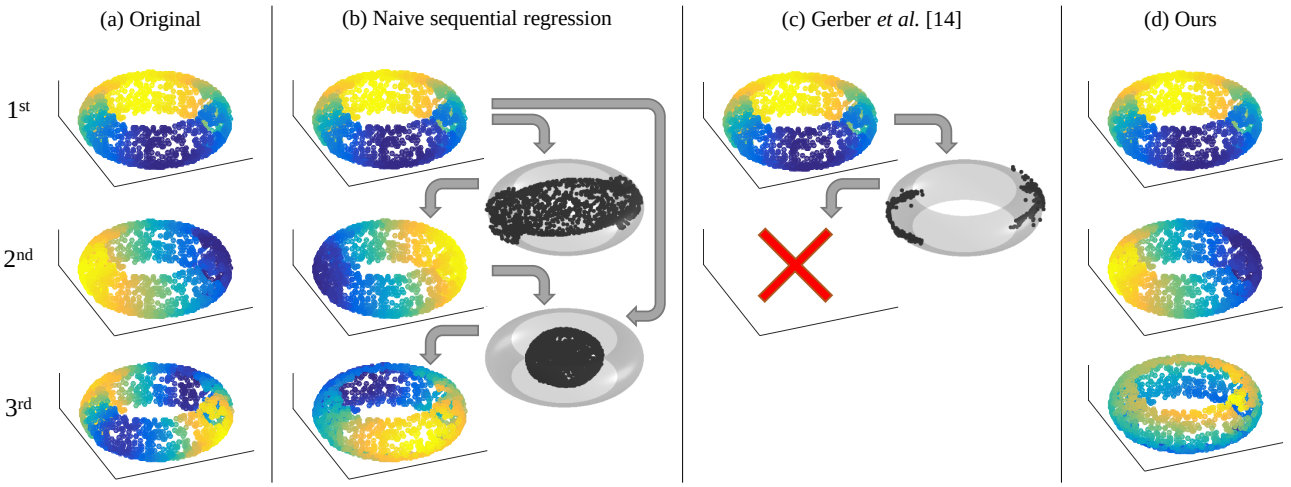

Figure 3. (a) The first three projections of points lying on a ring manifold, obtained with the original LEM algorithm. The projections correspond to $\cos(\theta)$, $\sin(\theta)$ and $\sin(2\theta + c)$, where θ is the outer angle of the ring. In this case, Projection 2 is not a function of Projection 1 and is thus non-redundant. But Projection 3 is a function of Projections 1 and 2, and is thus redundant. (b) The projections obtained with the naive sequential regression approach (Sec. 2). Here, Projection 3 is still redundant. The right column shows the points after subtracting their prediction from previous projections, which causes them to fall off the manifold. (c) The projections obtained with the algorithm of [14]. Here, the algorithm halts after one projection. The right column shows the points after the advection process along the manifold, which results in two clusters forming an unconnected graph. (d) The projections obtained with our non-redundant version of LEM. Our algorithm extracts a non-redundant third projection, which captures progression along the inner angle of the ring.

regressed against all previous ones (using some nonparametric regression method). Projections with low regression errors (*i.e*. which can be accurately predicted from the preceding ones) are discarded. This approach is quite efficient but usually works well only in simple situations. Its key limitation is that it is restricted to choose the projections from a given finite set of functions, which may not necessarily contain a "good" subset. Indeed, as we demonstrate in Sec. 5.2, in real-world high-dimensional settings all the projections tend to be partially predictable from previous ones. Yet, there usually does not exist any single projection which can be considered fully redundant. Therefore, despite the obvious dependencies, almost no projection is practically discarded in this approach.

To overcome this drawback, one could attempt to compute the projections sequentially, by eliminating the variations in the data which can be attributed to the projections that have already been computed. A naive way of doing so, would be to subtract from the data points their predictions based on all the previous projections. However, perhaps counter-intuitively, this *sequential regression* process does not necessarily prevent redundancy. The reason is that the data points may fall off the manifold during the iterations, as demonstrated in Fig. 3(b).

A more sophisticated approach, suggested by Gerber *et al*. [14], is to collapse the data points *along the manifold* in the direction of the gradient of the previous projection. In this approach, the points always remain on the manifold. However, this method fails whenever a projection is a non-monotonic function of some coordinate along the manifold. This happens, for example, in the ring manifold of Fig. 3. In this case, the first projection extracted by LEM corresponds to $\cos(\theta)$, where θ is the outer angle of the ring. Therefore, before computing the second projection, the advection process moves the points along the θ coordinate towards the locations at which $\cos(\theta)$ attains its mean value, which is 0. This causes the points with $\theta \in (0, \pi)$ to collapse to $\theta = \pi/2$, and the points with $\theta \in (\pi, 2\pi)$ to collapse to $\theta = 3\pi/2$. The two resulting clusters form an unconnected graph, so that LEM cannot be applied once more. An additional drawback of this method is that it requires a-priori knowledge of the manifold dimension. Furthermore, it is very computationally intensive and thus impractical for high-dimensional big data applications.

In this paper, we propose a different approach. Similarly to the methods described above, our algorithm is sequential. However, rather than heuristically modifying the data points in each stage, we propose to directly incorporate constraints which guarantee that the projections are not redundant.

3. Eliminating Redundancy

Nonlinear dimensionality reduction algorithms seek a set of *non-linear* projections $f_i : \mathbb{R}^D \rightarrow \mathbb{R}$, $i = 1, \cdots, d$ which map D-dimensional data points $\boldsymbol{x}_n \in \mathbb{R}^D$ into a d-

dimensional feature space ($d < D$).

Definition 3.1 *We call a sequence of projections $\{f_i\}$* ***non-redundant*** *if none of them can be expressed as a function of the preceding ones. That is, for every i,*

$$f_i(\boldsymbol{x}) \neq g(f_{i-1}(\boldsymbol{x}), \cdots, f_1(\boldsymbol{x})) \tag{3}$$

for every (possibly nonlinear) function $g : \mathbb{R}^{i-1} \to \mathbb{R}$.

Let us see why existing spectral dimensionality reduction algorithms do not necessarily yield non-redundant projections. Spectral algorithms obtain the ith projection of all the data points, denoted by $\boldsymbol{f}_i = (f_i(\boldsymbol{x}_1), \cdots, f_i(\boldsymbol{x}_N))^T$, as the solution to the optimization problem[1]

$$\begin{aligned} \max_{\boldsymbol{f}_i} \quad & \boldsymbol{f}_i^T \boldsymbol{K} \boldsymbol{f}_i \\ \text{s.t.} \quad & \mathbf{1}^T \boldsymbol{f}_i = 0 \\ & \boldsymbol{f}_i^T \boldsymbol{f}_i = 1 \\ & \boldsymbol{f}_i^T \boldsymbol{f}_j = 0, \quad \forall j < i. \end{aligned} \tag{4}$$

Here, $\mathbf{1}$ is an $N \times 1$ vector of ones and $\boldsymbol{K}$ is an $N \times N$ algorithm-specific positive definite (kernel) matrix, constructed from the data points [16, 36]. The first constraint in Problem (4) ensures that the projections have zero means. The last two constraints restrict the projections to have unit norms and to be orthogonal w.r.t. one another. The solution to Problem (4) is given by the d top eigenvectors of the centered kernel matrix $(\boldsymbol{I} - \frac{1}{N}\mathbf{1}\mathbf{1}^T)\boldsymbol{K}(\boldsymbol{I} - \frac{1}{N}\mathbf{1}\mathbf{1}^T)$. When $\boldsymbol{K}$ is a stochastic matrix (*e.g.* LLE, LEM), the solution is simply eigenvectors $2, \ldots, d+1$ of $\boldsymbol{K}$ (without centering).

The orthogonality constraints in Problem (4) guarantee that the projections be linearly independent. However, these constraints do not guarantee non-redundancy. To see this, it is insightful to interpret them in statistical terms. Assume that the data points $\{\boldsymbol{x}_n\}$ correspond to independent realizations of some random vector X. Then orthogonality corresponds to zero statistical correlation, as

$$\mathbb{E}\left[f_i(X) f_j(X)\right] \approx \tfrac{1}{N} \sum_n f_i(\boldsymbol{x}_n) f_j(\boldsymbol{x}_n) = \tfrac{1}{N} \boldsymbol{f}_i^T \boldsymbol{f}_j. \tag{5}$$

Therefore, in particular, the orthogonality constraints in (4) guarantee that each projection be uncorrelated with any linear combination of the preceding projections. This implies that $f_i(X)$ *cannot be a linear function of the previous projections* $\{f_j(X)\}_{j<i}$. However, this does not imply that $f_i(X)$ cannot be a *nonlinear* function of the previous projections (which would lead to redundancy, as we saw in figs. 1 and 2).

[1] Note that LEM and DFM use slightly different constraints (see Appendix A.1). Also, note that some methods (*e.g.* LEM, LLE) rather *minimize* the objective in (4). Here we address only the maximization problem, as minimizing $\boldsymbol{f}_i^T \boldsymbol{K} \boldsymbol{f}_i$ is equivalent to maximizing $\boldsymbol{f}_i^T \check{\boldsymbol{K}} \boldsymbol{f}_i$, where $\check{\boldsymbol{K}} = \lambda_{\max} \boldsymbol{I} - \boldsymbol{K}$ with $\lambda_{\max}$ denoting the largest eigenvalue of $\boldsymbol{K}$ [19, 3].

To enforce non-redundancy, we propose to use the following observation.

Lemma 3.2 *A sequence of zero-mean projections $\{f_i\}$ is* ***non-redundant*** *if each of them is* ***unpredictable*** *from the preceding ones, namely*

$$\mathbb{E}\left[f_i(X) | f_{i-1}(X), \cdots, f_1(X)\right] = 0. \tag{6}$$

To see this, note that according to the orthogonality property of the conditional expectation,

$$\begin{aligned} \mathbb{E}\Big[\Big(f_i(X) - \mathbb{E}[f_i(X) | f_{i-1}(X), \cdots, f_1(X)]\Big) \\ \times g(f_{i-1}(X), \cdots, f_1(X))\Big] = 0 \end{aligned} \tag{7}$$

for every function g. Now, if we substitute (6), we get that

$$\mathbb{E}\left[f_i(X)\, g(f_{i-1}(X), \cdots, f_1(X))\right] = 0, \quad \forall g. \tag{8}$$

Namely, $f_i(X)$ must be uncorrelated with every (not necessarily linear) function of the previous projections. This implies that $f_i(X)$ cannot be a function of the preceding projections. Thus, by definition, the projections are non-redundant in this case.

4. Algorithm

The unpredictability condition (6) is in fact an infinite set (a continuum) of constraints, as it restricts the conditional expectation of $f_i(X)$ to be zero, given every possible value that the previous projections $\{f_j(X)\}_{j<i}$ may take. To obtain a practical method, we propose to enforce these restrictions only at the embedding points of the data samples, leading to a discrete set of N constraints. To do this, we construct a kernel smoother matrix $\boldsymbol{P}_i$ (*e.g.* the Nadaraya-Watson estimator [26, 39]) for regressing $\boldsymbol{f}_i$ against $\boldsymbol{f}_{i-1}, \ldots, \boldsymbol{f}_1$, so that the nth entry of the vector $\boldsymbol{P}_i \boldsymbol{f}_i$ constitutes an approximation to the conditional expectation of $f_i(X)$ given that $f_{i-1}(X) = f_{i-1}(x_n), \ldots, f_1(X) = f_1(x_n)$. With this construction, we can replace the zero-correlation constraints $\boldsymbol{f}_i^T \boldsymbol{f}_j = 0$ in (4), by the unpredictability restrictions $\boldsymbol{P}_i \boldsymbol{f}_i = \mathbf{0}$.

Note, however, that $\boldsymbol{P}_i$ will generally be a full-rank matrix so that the constraint $\boldsymbol{P}_i \boldsymbol{f}_i = \mathbf{0}$ would generally be satisfied only by the trivial solution $\boldsymbol{f}_i = \mathbf{0}$. Nonetheless, the singular values of $\boldsymbol{P}_i$ typically decay sharply and become negligible from some point on. We can thus safely replace $\boldsymbol{P}_i$ by its low-rank approximation $\boldsymbol{P}_i^r = \boldsymbol{U}_i^r \boldsymbol{D}_i^r (\boldsymbol{V}_i^r)^T$ (corresponding to the top r terms in its singular value decomposition), given that we choose the rank r large enough. Our proposed redundancy-avoiding version of the spectral

Algorithm 1 Non-redundant dimensionality reduction.

Input: High-dimensional data points $\boldsymbol{x}_n \in \mathbb{R}^D$.
Output: Embeddings $\boldsymbol{f}_i = (f_i(\boldsymbol{x}_1), \cdots, f_i(\boldsymbol{x}_N))^T$.

1: Construct the kernel matrix $\boldsymbol{K}$ as in the original algorithm (*e.g.* LLE, LEM, Isomap, etc.).
2: If the original algorithm *minimizes* the objective of (4) (*e.g.* LLE, LEM), then set $\boldsymbol{K} \leftarrow \lambda_{\max}\boldsymbol{I} - \boldsymbol{K}$.
3: Assign the top (non-trivial) eigen-vector of $\boldsymbol{K}$ to $\boldsymbol{f}_1$.
4: **for** $i = 2, \ldots, d$ **do**
5: Construct smoothing matrix

$$[\boldsymbol{P}_i]_{j,k} \leftarrow \exp\left\{-\frac{\sum_{\ell=1}^{i-1}\left(f_\ell\left(x_j\right) - f_\ell\left(x_k\right)\right)^2}{2h^2}\right\},$$

$$[\boldsymbol{P}_i]_{j,k} \leftarrow \frac{[\boldsymbol{P}_i]_{j,k}}{\sum_{n=1}^{N}[\boldsymbol{P}_i]_{j,n}}.$$

6: Compute $\boldsymbol{V}_i^r \in \mathbb{R}^{N\times r}$, the top r right singular vectors of $\boldsymbol{P}_i$.
7: Form the modified kernel matrix

$$\tilde{\boldsymbol{K}}_i \leftarrow \left(\boldsymbol{I} - \boldsymbol{V}_i^r(\boldsymbol{V}_i^r)^T\right)\boldsymbol{K}\left(\boldsymbol{I} - \boldsymbol{V}_i^r(\boldsymbol{V}_i^r)^T\right).$$

8: Assign the top eigen-vector of $\tilde{\boldsymbol{K}}_i$ to $\boldsymbol{f}_i$.
9: **end for**

dimensionality reduction problem (4) is therefore

$$\begin{aligned} \max_{\boldsymbol{f}_i} \quad & \boldsymbol{f}_i^T\boldsymbol{K}\boldsymbol{f}_i \\ \text{s.t.} \quad & \mathbf{1}^T\boldsymbol{f}_i = 0 \\ & \boldsymbol{f}_i^T\boldsymbol{f}_i = 1 \\ & \boldsymbol{P}_i^r\boldsymbol{f}_i = \mathbf{0}, \quad \forall i > 1. \end{aligned} \tag{9}$$

The solution to this new problem is no longer given by the spectral decomposition of $\boldsymbol{K}$. However, it can be brought into a convenient form by using the following lemma[2] (see proof in Appendix A.2).

Lemma 4.1 *The vectors $\boldsymbol{f}_1, \ldots, \boldsymbol{f}_d$ which optimize Problem (9), also optimize*

$$\begin{aligned} \max_{\boldsymbol{f}_i} \quad & \boldsymbol{f}_i^T\tilde{\boldsymbol{K}}_i\boldsymbol{f}_i \\ \text{s.t.} \quad & \mathbf{1}^T\boldsymbol{f}_i = 0 \\ & \boldsymbol{f}_i^T\boldsymbol{f}_i = 1, \end{aligned} \tag{10}$$

where $\tilde{\boldsymbol{K}}_i = (\boldsymbol{I} - \boldsymbol{V}_i^r(\boldsymbol{V}_i^r)^T)\boldsymbol{K}(\boldsymbol{I} - \boldsymbol{V}_i^r(\boldsymbol{V}_i^r)^T)$ with $\boldsymbol{V}_i^r$ denoting the top r right singular vectors of $\boldsymbol{P}_i$ and $\boldsymbol{V}_1^r = \mathbf{0}$.

From this lemma, it becomes clear that $\boldsymbol{f}_i$ is precisely the top eigenvector of $\tilde{\boldsymbol{K}}_i$. This implies that we can determine the non-redundant projections sequentially. In the ith step, we first modify the kernel $\boldsymbol{K}$ according to the previous projections $\boldsymbol{f}_{i-1}, \ldots, \boldsymbol{f}_1$ to obtain $\tilde{\boldsymbol{K}}_i$. Then, we compute its top eigenvector to obtain projection $\boldsymbol{f}_i$. This is summarized in Alg. 1, where for concreteness, we chose $\boldsymbol{P}_i$ to be the Nadaraya-Watson smoother with a Gaussian-kernel.

[2]Note that this lemma holds true only for *maximization* problems.

4.1. Efficient implementation

In several spectral dimensionality reduction algorithms (*e.g.* LLE, LEM) the kernel matrix $\boldsymbol{K}$ is sparse, making them fit for large data sets in terms of memory and computational requirements. However, our modified kernel matrices $\tilde{\boldsymbol{K}}_i$ are generally not sparse. To retain some of the efficiency of the original algorithms, we make two adjustments to Alg. 1. First, in step 5 of the algorithm, we construct a *sparse* smoothing matrix $\boldsymbol{P}_i$, by using only the k nearest neighbors of each sample. This reduces the memory required to store $\boldsymbol{P}_i$ and also enables efficient computation of its top r singular vectors $\boldsymbol{V}_i^r$ (step 6). Second, we use the fast method of [18] to compute the top eigenvector of $\tilde{\boldsymbol{K}}_i$ (step 8). Besides speed, this has the advantage that we never need to explicitly form the dense matrix $\tilde{\boldsymbol{K}}_i$ (step 7). Indeed, each iteration of [18] involves multiplication by $\tilde{\boldsymbol{K}}_i$, which can be broken into multiplications by $\boldsymbol{V}_i^r$, $(\boldsymbol{V}_i^r)^T$, and $\boldsymbol{K}$. Therefore, we only have to store $\boldsymbol{K}$, which is sparse, and $\boldsymbol{V}_i^r$, which is $N \times r$ with $r \ll N$.

It should be noted, however, that the effect of the sparsity of $\boldsymbol{P}_i$ on the running time and memory use, is somewhat more modest than could be expected. This is because the sparser $\boldsymbol{P}_i$ is, the slower its singular values decay, and thus the larger the rank r is required to be. Thus, a sparser $\boldsymbol{P}_i$ requires computation of more singular vectors, which also slows the eigen-decomposition of $\tilde{\boldsymbol{K}}_i$ (as $\boldsymbol{V}_i^r$ has more columns).

5. Experiments

We tested our non-redundant algorithm on three high-dimensional data sets. In all our experiments, we report results with the Nadaraya-Watson smoother [26, 39], as specified in Alg. 1. We also experimented with a locally linear smoother and did not observe a significant difference. The threshold for the low-rank approximation of the smoothing matrix was set to 3% of the largest singular value. We used the largest number of nearest neighbors such that $\boldsymbol{P}_i$ could still be stored in memory (10000 in our case).

5.1. Artificial head images

The artificial head image dataset [35] is a popular test bed for manifold learning techniques. It contains 64×64 computer-rendered images of a head, with varying vertical and horizontal camera positions (denoted by θ and ϕ) and lighting directions (denoted by ψ). Since each of the parameters (θ, ϕ, ψ) varies significantly across this data set, most

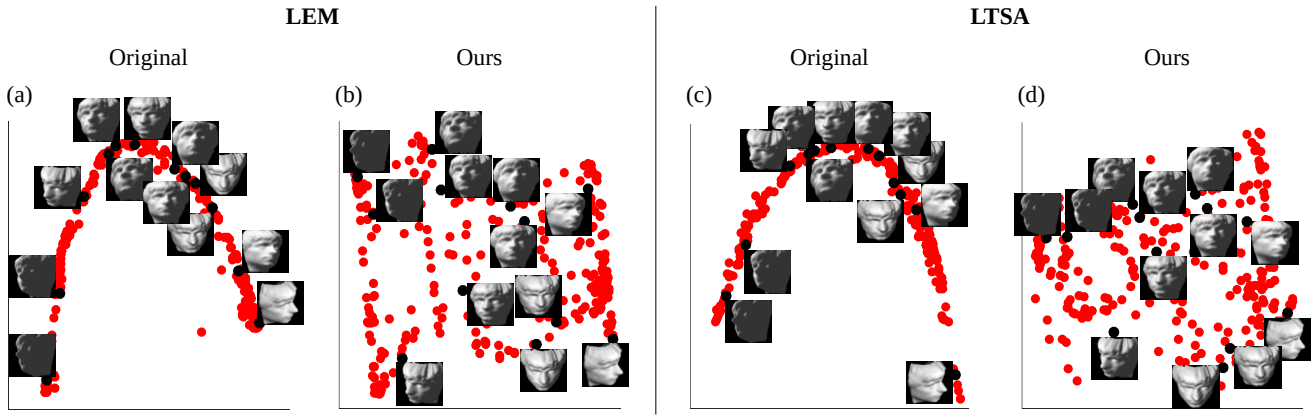

Figure 4. Two-dimensional embeddings of computer rendered face images with varying vertical angles, horizontal angles, and lighting directions. (a) The original LEM method. (b) Our non-redundant LEM. (c) The original LTSA method. (d) Our non-redundant LTSA. The original algorithms produce redundant representations, as their second coordinate is a function of the first. In our method, the second coordinate clearly carries additional information w.r.t. first, and therefore our representations are non-redundant.

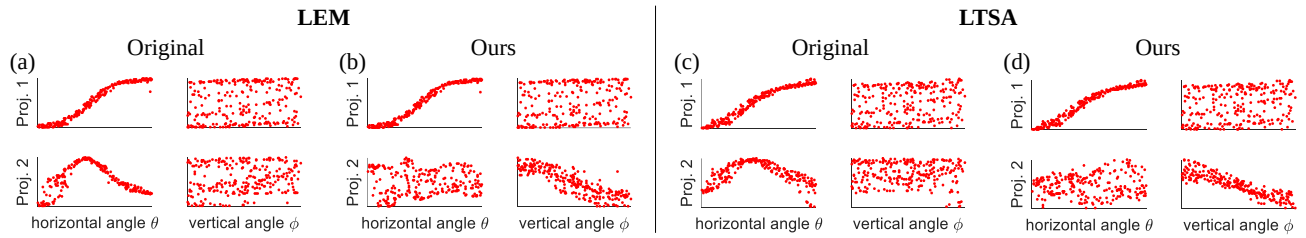

Figure 5. The first two projections of the head images of Fig. 4 vs. the horizontal and vertical angles (θ, ϕ) of the heads. (a) The original LEM method. (b) Our non-redundant LEM. (c) The original LTSA method. (d) Our non-redundant LTSA. The two projections extracted by the original algorithms are *both* correlated only with the horizontal angle θ. In our non-redundant algorithms, on the other hand, the second projection is correlated with the vertical angle ϕ.

spectral methods manage to non-redundantly extract those parameters with the first three projections.

Here, to make the representation learning task more challenging, we chose a 257 subset of the original data set, corresponding to the reduced parameter range $\theta \in [-75°, 75°]$, $\phi \in [-8°, 8°]$, $\psi \in [105°, 175°]$. Figures 4(a),(c) visualize the projections extracted by LEM and LTSA in this case. As can be seen, both algorithms produce redundant representations, as their second projection is a deterministic function of the first. When incorporating our unpredictability constraints, we are able to avoid this repetition, as evident from figs. 4(b),(d). Indeed, in our method, the second projection clearly carries additional information w.r.t. the first.

To analyze what the projections capture, we plot in Fig. 5 each of the embedding coordinates vs. the horizontal and vertical camera positions. From figs. 5(a),(c) it becomes obvious that in the original algorithms, Projections 1 and 2 are both correlated only with the horizontal angle θ. In our approach, on the other hand, Projection 1 captures the horizontal angle θ while Projection 2 reveals the vertical angle ϕ (see figs. 5(b),(d)).

5.2. MNIST handwritten digits

In most practical applications, the "correct" parametrization of the data manifold is not as obvious as in the head experiment. One such example is the MNIST database [22], which contains 28×28 images of handwritten digits. In such settings, determining the quality of a low-dimensional representation can be done by measuring its impact on the performance in downstream tasks, like classification.

In the next experiment, we randomly chose a subset of 15K images from the MNIST data set, based on which we learned low-dimensional representations with LEM and with three modifications of LEM: (i) our non-redundant method, (ii) the sequential regression technique (Sec. 2), (iii) the algorithm of Dsilva *et al.* [10]. We then split the data into 10K/2.5K/2.5K for training/tuning/testing and trained a third degree polynomial-kernel SVM [6] to classify the digits based on their low-dimensional representations. The SVM's soft margin parameter c and kernel parameter γ were tuned based on performance on the tune set (within the range $c \in [1, 10]$, $\gamma \in [0.1, 0.2]$). Fig. 6(a) shows the classification error vs. the representation dimen-

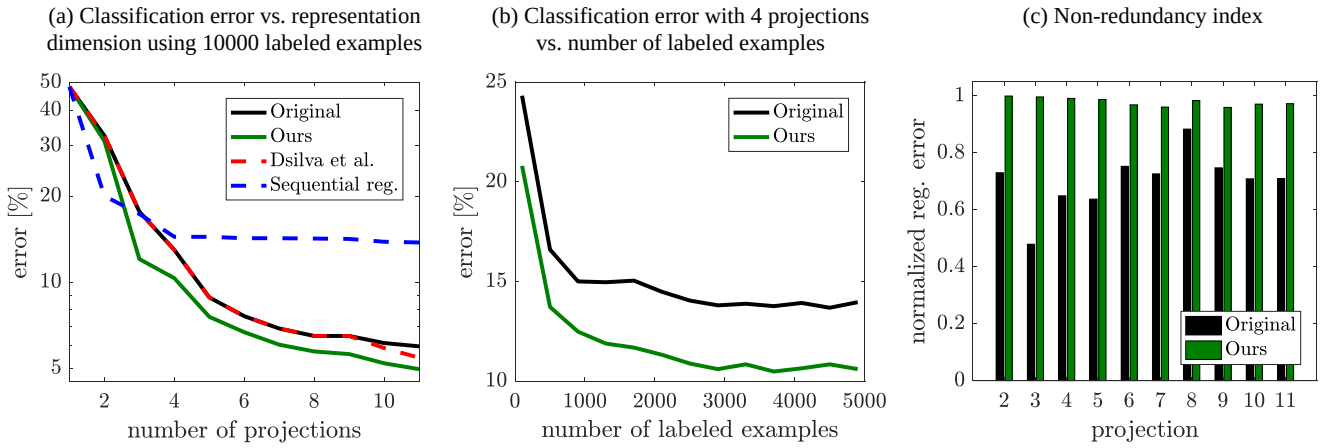

Figure 6. An SVM classifier was trained on low-dimensional representations of handwritten digit images obtained with LEM, our non-redundant LEM, and two additional approaches (see Sec. 2). (a) Classification error vs. the representation dimension. (b) Classification error vs. the number of examples used to train the SVM (with a fixed four-dimensional representation). (c) Normalized errors attained in regressing each projection against all previous ones. Low errors indicate that the corresponding projections are redundant.

sionality for each of the algorithms. As can be seen, our non-redundant representation leads to the largest and most consistent decrease in the classification error.

An additional benefit of having a non-redundant representation, is that it allows to achieve the same performance (or better) with fewer training examples. This is illustrated in Fig. 6(b), where we plot the classification error with a four-dimensional representation vs. the number of examples used to train the SVM. As can be seen, our method requires only 400 labeled examples to achieve a lower error than the original LEM with 5000 samples. This feature is extremely useful in semi-supervised settings with many unlabeled examples (which can be used to learn a good representation), and only a few labeled samples (which are enough for learning a good classifier when the representation is good).

Recall that the algorithm of [10] constructs its representation by choosing among the projections of the original LEM. To see why this does not lead to significant improvement, we plot in Fig. 6(c) the normalized errors attained in regressing each projection against all previous ones. As suggested in [10], these errors indicate the extent to which the projections are redundant (lower is more redundant, see Sec. 2). Notice that in the original LEM, all the projections are somewhat redundant (their errors are lower than 100%). However, they clearly carry additional information (the errors are not close to 0%) and thus cannot be considered fully redundant. Consequently, almost none of them are discarded in the method of [10]. In contrast, our algorithm produces projections which cannot be predicted from the previous ones (with errors $\sim$100%). Therefore, with the same number of dimensions, we are able to preserve more information about the data.

5.3. Image patch representation

Finally, to visualize the effect of non-redundancy in low-level vision tasks, we extracted all 7×7 patches with 3 pixel overlap from an image (taken from [31]), and learned a three dimensional representation using Isomap and using our non-redundant version of Isomap. Figure 7 visualizes the first three projections by coloring each pixel according to the embedding value of its surrounding patch. Observe that in the original algorithm, the first projection captures brightness, the second redundantly captures brightness once more, and the third captures mainly vertical edges with some brightness attributes still remaining (*e.g.* the sky, the left poolside). In contrast, in our algorithm, the second and third projections capture the vertical *and horizontal* edges (without redundantly capturing brightness multiple times), thus providing additional information.

6. Conclusions

We presented a general approach for overcoming the redundancy phenomenon in spectral dimensionality reduction algorithms. As opposed to prior attempts, which fail in complex high-dimensional situations, our approach provably produces non-redundant representations. This is achieved by replacing the orthogonality constraints underlying spectral methods, by unpredictability constraints. Our solution reduces to applying a sequence of spectral decompositions, where in each step, the kernel matrix is modified according to the projections computed so far. Our experiments clearly illustrate the ability of our method to capture more informative compact representations of high-dimensional data.

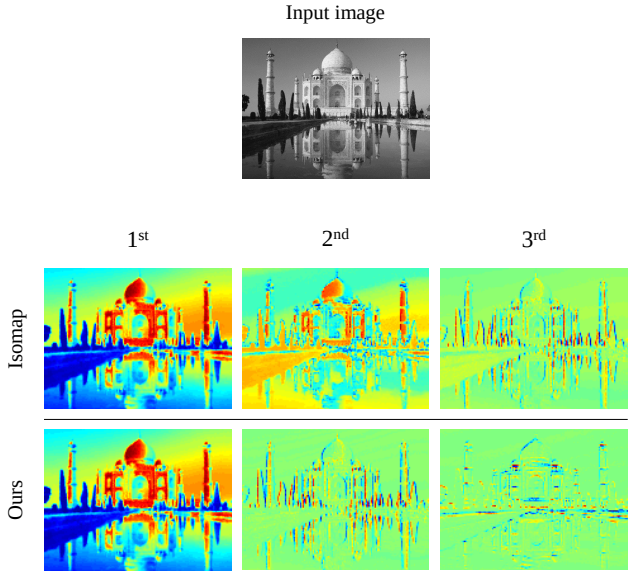

Figure 7. Three-dimensional embedding of all 7×7 patches with a 3 pixel overlap, obtained with Isomap and with our non-redundant version of Isomap. Each pixels is colored according to the projection of its surrounding patch. In both methods, the first projection captures brightness. However, the original Isomap redundantly captures brightness-related features again with the second projection, and captures vertical edges only with the third projection. In contrast, our non-redundant version captures vertical *and horizontal* edges with the second and third projections.

A. Detailed proofs and Remarks

A.1. Optimization Problem (4) for LEM and DFM

In the case of LEM and DFM, the objective $\boldsymbol{f}_i^T \boldsymbol{K} \boldsymbol{f}_i$ is optimized s.t. the constraints $\boldsymbol{f}_i^T \boldsymbol{D} \boldsymbol{f}_j = \delta_{i,j}$ and $\mathbf{1}^T \boldsymbol{D} \boldsymbol{f}_i = 0$, where $\boldsymbol{D}$ is a diagonal matrix with entries $[\boldsymbol{D}]_{i,i} = \sum_j [\boldsymbol{K}]_{i,j}$. Similarly to (5), these constraints can be interpreted as restrictions on the *weighted* means and *weighted* correlations between the projections. Namely, $E[f_i(X)d(X)] = 0$ and $E[f_i(X)f_j(X)d(X)] = 0$, where $d(x) = \int k(x,y)dy$. Accordingly, we define non-redundancy in this case as zero weighted correlation between each projection and *any function* of the previous projections. That is, for each i, we would like to ensure that $\mathbb{E}[f_i(X)g(f_{i-1}(X), \cdots, f_1(X))d(X)] = 0$ for every function g (analogously to (8)). This is equivalent to the requirement that $\mathbb{E}[f_i(X)d(X)|f_{i-1}(X), \cdots, f_1(X)] = 0$, which we approximate at the data points by $\boldsymbol{P}_i \boldsymbol{D} \boldsymbol{f}_i = \mathbf{0}$.

By denoting $\hat{\boldsymbol{f}}_i = \boldsymbol{D}^{\frac{1}{2}} \boldsymbol{f}_i$, $\hat{\boldsymbol{K}} = \boldsymbol{D}^{-\frac{1}{2}} \boldsymbol{K} \boldsymbol{D}^{-\frac{1}{2}}$ and $\hat{\boldsymbol{P}}_i = \boldsymbol{P}_i \boldsymbol{D}^{\frac{1}{2}}$, the corresponding optimization problem becomes

$$\begin{aligned} \min/\max_{\hat{\boldsymbol{f}}_i} \quad & \hat{\boldsymbol{f}}_i{}^T \hat{\boldsymbol{K}} \hat{\boldsymbol{f}}_i \\ \text{s.t.} \quad & \hat{\boldsymbol{f}}_i{}^T \hat{\boldsymbol{f}}_i = 1 \\ & \hat{\boldsymbol{P}}_i^r \hat{\boldsymbol{f}}_i = \mathbf{0}, \quad \forall i > 1, \end{aligned} \tag{11}$$

where min/max corresponds to LEM/DFM respectively. Therefore, to obtain a non-redundant version of these algorithms, we simply apply Alg. 1 with $\hat{\boldsymbol{K}}$ and $\hat{\boldsymbol{P}}_i$ rather than with $\boldsymbol{K}$ and $\boldsymbol{P}_i$, and then multiply the extracted projections by $\boldsymbol{D}^{-\frac{1}{2}}$ from the left. Notice that to form the regression matrix $\boldsymbol{P}_i$, we use $\{\boldsymbol{f}_j\}$, and not $\{\hat{\boldsymbol{f}}_j\}$.

A.2. Proof of lemma 4.1

We start by proving that any $\boldsymbol{f}_i$ solving (10) necessarily satisfies $\boldsymbol{P}_i^r \boldsymbol{f}_i = \mathbf{0}$. First, note that this constraint is equivalent to $\boldsymbol{V}_i^r (\boldsymbol{V}_i^r)^T \boldsymbol{f}_i = \mathbf{0}$, as $\boldsymbol{D}_i^r$, $\boldsymbol{U}_i^r$, and $\boldsymbol{V}_i^r$ have empty null spaces. Now, suppose that $\boldsymbol{f}_i$ maximizes the objective of (10) and satisfies the constraints $\|\boldsymbol{f}_i\| = 1$ and $\mathbf{1}^T \boldsymbol{f}_i = \mathbf{0}$, but does not satisfy $\boldsymbol{V}_i^r (\boldsymbol{V}_i^r)^T \boldsymbol{f}_i = \mathbf{0}$. Then define the alternative solution

$$\tilde{\boldsymbol{f}}_i = \frac{(\boldsymbol{I} - \boldsymbol{V}_i^r (\boldsymbol{V}_i^r)^T) \boldsymbol{f}_i}{\|(\boldsymbol{I} - \boldsymbol{V}_i^r (\boldsymbol{V}_i^r)^T) \boldsymbol{f}_i\|}, \tag{12}$$

which clearly satisfies the constraints $\|\tilde{\boldsymbol{f}}_i\| = 1$ and $\mathbf{1}^T \tilde{\boldsymbol{f}}_i = \mathbf{0}$, but additionally also satisfies $\boldsymbol{V}_i^r (\boldsymbol{V}_i^r)^T \boldsymbol{f}_i = \mathbf{0}$. Notice that $\boldsymbol{I} - \boldsymbol{V}_i^r (\boldsymbol{V}_i^r)^T$ is a projection matrix (as $\boldsymbol{V}_i^r$ is orthogonal), so that

$$(\boldsymbol{I} - \boldsymbol{V}_i^r (\boldsymbol{V}_i^r)^T)^2 = \boldsymbol{I} - \boldsymbol{V}_i^r (\boldsymbol{V}_i^r)^T \tag{13}$$

and

$$\|(\boldsymbol{I} - \boldsymbol{V}_i^r (\boldsymbol{V}_i^r)^T) \boldsymbol{f}_i\|^2 \leq \|\boldsymbol{f}_i\|^2 = 1. \tag{14}$$

Therefore,

$$\begin{aligned} \tilde{\boldsymbol{f}}_i{}^T \tilde{\boldsymbol{K}}_i \tilde{\boldsymbol{f}}_i &= \frac{\boldsymbol{f}_i^T (\boldsymbol{I} - \boldsymbol{V}_i^r (\boldsymbol{V}_i^r)^T)^2 \boldsymbol{K} (\boldsymbol{I} - \boldsymbol{V}_i^r (\boldsymbol{V}_i^r)^T)^2 \boldsymbol{f}_i}{\|(\boldsymbol{I} - \boldsymbol{V}_i^r (\boldsymbol{V}_i^r)^T) \boldsymbol{f}_i\|^2} \\ &= \frac{\boldsymbol{f}_i^T \tilde{\boldsymbol{K}}_i \boldsymbol{f}_i}{\|(\boldsymbol{I} - \boldsymbol{V}_i^r (\boldsymbol{V}_i^r)^T) \boldsymbol{f}_i\|^2} \geq \boldsymbol{f}_i^T \tilde{\boldsymbol{K}}_i \boldsymbol{f}_i \end{aligned} \tag{15}$$

with equality only when $\boldsymbol{V}_i^r (\boldsymbol{V}_i^r)^T \boldsymbol{f}_i = \mathbf{0}$. In other words, $\tilde{\boldsymbol{f}}_i$ achieves a higher objective value than $\boldsymbol{f}_i$, contradicting our assumption that $\boldsymbol{f}_i$ is a solution to (10). This proves that any $\boldsymbol{f}_i$ that solves problem (10) necessarily also satisfies the constraints of problem (9). Therefore, effectively, the solutions to (9) and (10) satisfy the same constraints.

Next, observe that if $\boldsymbol{f}_i$ satisfies the constraint $\boldsymbol{V}_i^r (\boldsymbol{V}_i^r)^T \boldsymbol{f}_i = \mathbf{0}$ then the objectives of (9) and (10) are equivalent, since

$$\begin{aligned} \boldsymbol{f}_i^T \tilde{\boldsymbol{K}}_i \boldsymbol{f}_i &= \boldsymbol{f}_i^T (\boldsymbol{I} - \boldsymbol{V}_i^r (\boldsymbol{V}_i^r)^T) \boldsymbol{K} (\boldsymbol{I} - \boldsymbol{V}_i^r (\boldsymbol{V}_i^r)^T) \boldsymbol{f}_i \\ &= \boldsymbol{f}_i^T \boldsymbol{K} \boldsymbol{f}_i. \end{aligned} \tag{16}$$

Therefore, $\boldsymbol{f}_i$ solves (10) if and only if it solves (9).

References

[1] M. Belkin and P. Niyogi. Laplacian eigenmaps for dimensionality reduction and data representation. *Neural Computation*, 15(6):1373–1396, 2003. 1

[2] M. Belkin and P. Niyogi. Semi-supervised learning on Riemannian manifolds. *Machine Learning*, 56(1-3):209–239, 2004. 1

[3] Y. Bengio, J.-F. Paiement, P. Vincent, O. Delalleau, N. Le Roux, and M. Ouimet. Out-of-sample extensions for LLE, Isomap, MDS, Eigenmaps, and Spectral Clustering. *Advances in Neural Information Processing Systems (NIPS)*, 16:177–184, 2004. 1, 4

[4] A. Brun, H.-J. Park, H. Knutsson, and C.-F. Westin. Coloring of DT-MRI fiber traces using Laplacian eigenmaps. In *International Conference on Computer Aided Systems Theory*, pages 518–529, 2003. 1

[5] A. Chakrabarti, A. Rajagopalan, and R. Chellappa. Super-resolution of face images using kernel PCA-based prior. *IEEE Transactions on Multimedia*, 9(4):888–892, 2007. 1

[6] C.-C. Chang and C.-J. Lin. LIBSVM: a library for support vector machines. *ACM Transactions on Intelligent Systems and Technology (TIST)*, 2(3):27, 2011. 6

[7] H. Chang, D.-Y. Yeung, and Y. Xiong. Super-resolution through neighbor embedding. In *IEEE Conference on Computer Vision and Pattern Recognition (CVPR)*, volume 1, pages I–I, 2004. 1

[8] R. R. Coifman and S. Lafon. Diffusion maps. *Applied and Computational Harmonic Analysis*, 21(1):5–30, 2006. 1

[9] D. L. Donoho and C. Grimes. Hessian eigenmaps: Locally linear embedding techniques for high-dimensional data. *Proceedings of the National Academy of Sciences*, 100(10):5591–5596, 2003. 1

[10] C. J. Dsilva, R. Talmon, R. R. Coifman, and I. G. Kevrekidis. Parsimonious representation of nonlinear dynamical systems through manifold learning: A chemotaxis case study. *Applied and Computational Harmonic Analysis*, 2015. 1, 2, 6, 7

[11] A. Elgammal and C.-S. Lee. Inferring 3d body pose from silhouettes using activity manifold learning. In *IEEE Conference on Computer Vision and Pattern Recognition (CVPR)*, volume 2, pages II–681, 2004. 1

[12] X. Geng, D.-C. Zhan, and Z.-H. Zhou. Supervised nonlinear dimensionality reduction for visualization and classification. *IEEE Transactions on Systems, Man, and Cybernetics, Part B (Cybernetics)*, 35(6):1098–1107, 2005. 1

[13] M. Georg, R. Souvenir, A. Hope, and R. Pless. Simultaneous data volume reconstruction and pose estimation from slice samples. In *IEEE Conference on Computer Vision and Pattern Recognition (CVPR)*, pages 1–6, 2008. 1

[14] S. Gerber, T. Tasdizen, and R. Whitaker. Robust non-linear dimensionality reduction using successive 1-dimensional Laplacian eigenmaps. In *International Conference on Machine Learning (ICML)*, pages 281–288, 2007. 1, 3

[15] A. Gisbrecht and B. Hammer. Data visualization by nonlinear dimensionality reduction. *Data Mining and Knowledge Discovery*, 5(2):51–73, 2015. 1

[16] Y. Goldberg, A. Zakai, D. Kushnir, and Y. Ritov. Manifold learning: The price of normalization. *The Journal of Machine Learning Research*, 9:1909–1939, 2008. 1, 2, 4

[17] G. Guo, Y. Fu, C. R. Dyer, and T. S. Huang. Image-based human age estimation by manifold learning and locally adjusted robust regression. *IEEE Transactions on Image Processing*, 17(7):1178–1188, 2008. 1

[18] N. Halko, P.-G. Martinsson, and J. A. Tropp. Finding structure with randomness: Probabilistic algorithms for constructing approximate matrix decompositions. *SIAM review*, 53(2):217–288, 2011. 5

[19] J. Ham, D. D. Lee, S. Mika, and B. Schölkopf. A kernel view of the dimensionality reduction of manifolds. In *International Conference on Machine Learning (ICML)*, page 47, 2004. 1, 4

[20] X. He, S. Yan, Y. Hu, P. Niyogi, and H.-J. Zhang. Face recognition using Laplacianfaces. *IEEE Transactions on Pattern Analysis and Machine Intelligence*, 27(3):328–340, 2005. 1

[21] P. Isola, D. Zoran, D. Krishnan, and E. H. Adelson. Crisp boundary detection using pointwise mutual information. In *European Conference on Computer Vision (ECCV)*, pages 799–814, 2014. 1

[22] Y. LeCun, L. Bottou, Y. Bengio, and P. Haffner. Gradient-based learning applied to document recognition. *Proceedings of the IEEE*, 86(11):2278–2324, 1998. 6

[23] C.-S. Lee and A. Elgammal. Modeling view and posture manifolds for tracking. In *International Conference on Computer Vision (ICCV)*, pages 1–8, 2007. 1

[24] H. Lim, O. I. Camps, M. Sznaier, and V. I. Morariu. Dynamic appearance modeling for human tracking. In *IEEE Conference on Computer Vision and Pattern Recognition (CVPR)*, volume 1, pages 751–757, 2006. 1

[25] I. S. Lim, P. de Heras Ciechomski, S. Sarni, and D. Thalmann. Planar arrangement of high-dimensional biomedical data sets by Isomap coordinates. In *IEEE Symposium on Computer-Based Medical Systems*, pages 50–55, 2003. 1

[26] E. A. Nadaraya. On estimating regression. *Theory of Probability & Its Applications*, 9(1):141–142, 1964. 4, 5

[27] S. Pang, D. Kim, and S. Y. Bang. Face membership authentication using SVM classification tree generated by membership-based LLE data partition. *IEEE Transactions on Neural Networks*, 16(2):436–446, 2005. 1

[28] R. Pless. Image spaces and video trajectories: Using Isomap to explore video sequences. In *International conference on Computer Vision (ICCV)*, volume 3, pages 1433–1440, 2003. 1

[29] B. Raytchev, I. Yoda, and K. Sakaue. Head pose estimation by nonlinear manifold learning. In *International Conference on Pattern Recognition (ICPR)*, volume 4, pages 462–466, 2004. 1

[30] S. T. Roweis and L. K. Saul. Nonlinear dimensionality reduction by locally linear embedding. *Science*, 290(5500):2323–2326, 2000. 1

[31] M. Rubinstein, D. Gutierrez, O. Sorkine, and A. Shamir. A comparative study of image retargeting. In *ACM Transactions on Graphics (TOG)*, volume 29, page 160, 2010. 7

[32] B. Schölkopf, A. Smola, and K.-R. Müller. Kernel principal component analysis. In *International Conference on Artificial Neural Networks (ICANN)*, pages 583–588, 1997. 1

[33] R. Souvenir and J. Babbs. Learning the viewpoint manifold for action recognition. In *IEEE Conference on Computer Vision and Pattern Recognition (CVPR)*, pages 1–7, 2008. 1

[34] R. Souvenir, Q. Zhang, and R. Pless. Image manifold interpolation using free-form deformations. In *IEEE International Conference on Image Processing (ICIP)*, pages 1437–1440, 2006. 1

[35] J. B. Tenenbaum, V. De Silva, and J. C. Langford. A global geometric framework for nonlinear dimensionality reduction. *Science*, 290(5500):2319–2323, 2000. 1, 5

[36] L. Van Der Maaten, E. Postma, and J. Van den Herik. Dimensionality reduction: a comparative review. *The Journal of Machine Learning Research*, 10:66–71, 2009. 1, 4

[37] M. Vlachos, C. Domeniconi, D. Gunopulos, G. Kollios, and N. Koudas. Non-linear dimensionality reduction techniques for classification and visualization. In *International Conference on Knowledge Discovery and Data Mining*, pages 645–651, 2002. 1

[38] Q. Wang, G. Xu, and H. Ai. Learning object intrinsic structure for robust visual tracking. In *IEEE Conference on Computer Vision and Pattern Recognition (CVPR)*, volume 2, pages II–227, 2003. 1

[39] G. S. Watson. Smooth regression analysis. *Sankhyā: The Indian Journal of Statistics, Series A*, pages 359–372, 1964. 4, 5

[40] Q. Zhang, R. Souvenir, and R. Pless. On manifold structure of cardiac MRI data: Application to segmentation. In *IEEE Conference on Computer Vision and Pattern Recognition (CVPR)*, volume 1, pages 1092–1098, 2006. 1

[41] Z. Zhang, T. W. Chow, and M. Zhao. Trace ratio optimization-based semi-supervised nonlinear dimensionality reduction for marginal manifold visualization. *IEEE Transactions on Knowledge and Data Engineering*, 25(5):1148–1161, 2013. 1

[42] Z.-y. Zhang and H.-y. Zha. Principal manifolds and nonlinear dimensionality reduction via tangent space alignment. *Journal of Shanghai University*, 8(4):406–424, 2004. 1